AI-Based PV Module Extraction And Hotspot Fault Detection Using Image Processing Technique

Jing Cheng Soh
School of Electrical and Electronic Engineering
Universiti Sains Malaysia, Engineering Campus
Pulau Pinang, Malaysia
jingcheng99@student.usm.my

Mohd Khairunaz bin Mat Desa
School of Electrical and Electronic Engineering
Universiti Sains Malaysia, Engineering Campus
Pulau Pinang, Malaysia
khairunaz@usm.my

***Abstract*— The growing demand of renewables leads to the rise of another problem, the maintenance of the system. PV module is inclusive as there are several conditions that may badly influence the efficiency. Thus, with the aid of thermal imaging, several stages had been set up to detect hotspots within the module, including module extraction through a YOLOv5 customized model, hotspot detection through statistical method and data visualization through graphical user interface. In the hotspot detection stage, the images were gone through image pre-processing to improve the quality. As a result, a module extraction model was successfully trained with an accuracy of 98% while the statistical method provided 85% accuracy for hotspot detection. An interface was also created for the user to observe results and perform manual operation in case of extraction failure.**

Keywords—PV, module extraction, hotspot detection, image processing, data visualization

I. INTRODUCTION

Renewable energy has been steadily dominating the current world's energy usage trend, reigning in an approximate 30% share of electricity production worldwide [1] . Contextually, renewable energy brings role-playing impacts on the reduction of carbon emissions, which is mainly responsible for drastic climate change, while serving as an alternative to the exhausting contaminating non-renewable energy. By comparing the global electricity demand between the first half of 2022 and 2021, an incremental usage of 389TWh, equivalent to a 3% increase, is found. The rising demand has been met by an increase in solar, wind, and hydro-generated power, preventing a 4% increase in fossil fuel generation, which may result in 230 million tons of CO2 emissions.

Statistics from International Energy Agency (IEA) forecasts that a record-breaking 300GW net renewable generating capacity addition will be achieved at the end of the year 2022. Among the 300GW capacity in 2022, PV's share achieves 59.1% with 71.1GW from distributed PV and 117.5GW from utility-scale PV [2].

The sustainability of photovoltaic (PV) modules faces significant challenges that need to be addressed for long-term viability. The main concerns of this issues include the high energy demand during the manufacturing process, the use of hazardous chemicals in the production of solar-grade silicon that poses environmental and health risks, and the future recycling of decommissioned solar panels that poses a growing challenge [3].

Adel Mellit has presented a novel approach for detecting and diagnosing faults in photovoltaic modules using thermographic images and deep convolutional neural networks (DCNNs). The database for DCNNs is collected using FLIR thermal camera and the images are augmented using Image Data Generator (IDG) algorithm, growing the database 20 times bigger. Two models are developed in this study, binary classification, and multi-classification. These models, after being developed, are optimized to fit them into an embedded system which is built around Raspberry Pi 4 [4].

Moath et al has proposed Super Linear Iterative Clustering (SLIC) algorithm in detecting faults in PV systems through thermography. The rough workflow of this study may be simplified into five steps. Firstly, thermal images of different defective PV modules are collected as input data. Then, the images are read into the system and converted into a compatible format. Next, super linear iterative clustering (SLIC) algorithm is applied to the images. Through the SLIC algorithm, the images are judged if the modules are defective. In case of detecting defective modules, input images are analyzed to determine the defect [5].

Luis E. Montanez et al has proposed an automatic detection by including two main stages in his paper, PV module segmentation and thermal analysis. The segmentation stage involves image pre-processing including the application of image transformation, dynamic histogram equalization and Gaussian filter, followed by adaptive thresholding using Otsu's method, and refining through the application of watershed transform. Thermal analysis begins by calculating the mean, standard deviation of the temperature. Then, the outliers, which fall away from a standard deviation away from the mean, are deemed hotspots. Visualization is performed by displaying the data in histogram on graphical user interface [6].

Masoud et al has presented an algorithm for detecting and localizing hotspot faults in PV systems using thermal images. Conversion of images into 1D pixel value is first conducted, followed by manual cropping the PV module in the image. Edge-preserving and smoothing filter is applied to remove the noise. Images are then converted to HSV format before masks with corresponding threshold values for HSV channels are slided into the images for hotspot detection. Permanent and transient hotspots are differentiated in this study using the concept of digital logic gate XOR [7].

Xiang Gao et al proposes a solar panel defect detection system that consists of two major components, panel recognition and defect detection. In the panel recognition stage, lines, corners, and contours are used as features. Firstly, the thermal images are smoothed using the Gaussian method, followed by edge detection through canny edge detection. Hough line transform is applied to detect a large number of line segments. The lines are then classified into two groups, vertical and horizontal. Corners and contours are the two additional features that help estimate lines in blurry frames. In the defect detection stage, local anomalies are detected using adaptive thresholding method whereas global anomalies are detected using DBSCAN method [8].

Feng Hong et al has proposed an effective way of detecting faulty modules using available algorithms, YOLOv5 and Resnet. Looking at the bigger picture, the framework of this study possesses seven steps, collecting visible and infrared images, importing images, segmenting PV modules from visual images using YOLOv5, obtaining corresponding infrared PV modules infrared images, detecting fault using Resnet, returning detected information to visible images and displaying fault warnings [9].

Last but not least, there are some other researchers that come out with different approaches to identify faults within PV module through thermal images. For instance, Muhammad Umair Ali et al has proposed a hybrid features-based support vector machine (SVM) model for PV modules classification and hotspot detection [10]. Also, the article written by Roberto Pierdicca et al proposes solAIr, a deep learning-based artificial intelligence system that detects anomalies in PV images obtained from unmanned aerial vehicles equipped with infrared radiation capturing devices [11].

Having the facts unfolded, the objectives of the paper are then set up to create an automated module extraction model based on YOLOv5 algorithm, detect faults within modules using thermal imaging, and create a graphical user interface to visualize the results.

II. METHODOLOGY

A. YOLOv5-based PV Module Extraction

The module extraction workflow is shown in the Fig.1. Image collection is first collected using FLIR Cx-series thermal camera to obtain both visual and thermal images from the same angle. Image pre-processing ensues by applying dynamic histogram equalization and Gaussian filter to enhance the image contrast and smooth the image respectively.

Image augmentation then takes place to increase the size of the database. Some augmentation technique may include flipping, rotating, cropping, changing pixel intensity, and so on. The probability of occurrence for each transformation is set to 0.5. By the end of augmentation stage, at least 500 image number shall be collected to achieve the minimum suggest number for customizing a model.

Image labelling is conducted by storing the bounding box coordinates of the PV module in the images in their corresponding text files. The storing format is in normalized 'xywh' format, indicating the center coordinates, width, and height of the bounding box respectively.

Having all the images labelled, the model is then trained by passing the images, and some other relevant information such as values of hyperparameters, and paths to the label text files to the YOLOv5.

Hyperparameters, including image resolution, batch size, and epochs are tuned to better the model accuracy. Upon achieving satisfactory accuracy, 90% and above, by testing the model with unseen data, the model is ready to be deployed for PV module extraction.

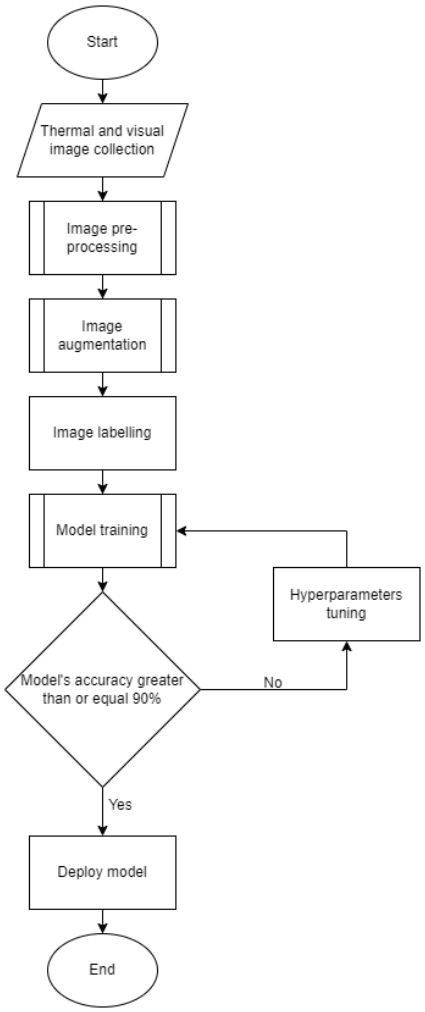

Fig.1. Module extraction model training workflow.

B. Development of Hotspot Detection Based On Statistics

Fig.2 illustrates the workflow of hotspot detection stage. First, at least 30 visual images are imported as the input based on central limit theorem. The PV modules within the images are extracted using the customized model. After obtaining the bounding box coordinates, the thermal images are then cropped according to the coordinates to remove the background.

Before analysis is carried out, image pre-processing is applied with grayscale conversion, contrast limited adaptive histogram equalization (CLAHE), and gaussian blurring. Grayscale conversion is done based on the equation below,

$$Grayscale = (0.299R + 0.587G + 0.114B)/3 \qquad (1)$$

Where R, G, and B represent the intensity value of red, green, and blue respectively. This aims to reduce the complexity of the information of three channels to one channel. CLAHE that serves to enhance the image contrast then ensues by applying the equation,

$$i_{new} = [\sum_{0}^{j=i} \frac{H(i)}{W \times H}] (L-1) \qquad (2)$$

To find the new intensity value for each pixel where H(i) is frequency of occurrence of the intensity value i, W and H are the image dimensions, and L is the maximum intensity

value in that image. After that, to reduce noise, Gaussian blurring is applied using the equation,

$$G(x,y) = \frac{1}{2\pi\sigma^2} e^{-\frac{x^2+y^2}{2\sigma^2}} \quad (3)$$

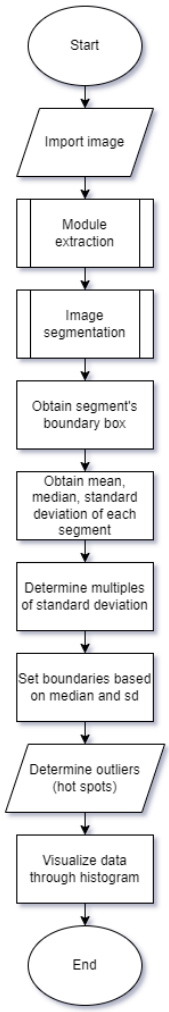

Fig.2. Hotspot detection workflow.

Where x and y represent the horizontal and vertical distance. σ symbol stands for standard deviation. Gaussian filter provides different weights to each entry in the matrix. Pixels that are closer to the selected pixel are granted greater weight and vice versa. To let this theory come into realization, the Gaussian function comes to the point as shown in the equation below.

Then, segmentation is carried out to divide the module image into 100 equal pieces for analysis. For every segment, the size is determined by,

$$Segment\ size = round(\frac{W \times H}{N_s^2}) \quad (4)$$

Where W and H are the image dimensions, and N_s indicates the number of rows or columns.

For every segment box, the mean is obtained. Using the means of the samples, the sample mean X, standard deviation σ, and median are calculated based on the equations,

$$mean, X = \frac{\sum_0^{m=N_I} i_m}{N_I} \quad (5)$$

$$standard\ deviation, \sigma = \sqrt{\frac{\sum(X - \mu)^2}{N_s}} \quad (6)$$

Then, trials and errors are executed to determine the optimum value of k multiplier in the equation to find the best fit of the upper boundary which is set up using the median and the standard deviation, to increase the accuracy of hotspot detection.

$$boundary = median \pm k\sigma \quad (7)$$

The outliers that fall outside of the boundary are deemed hotspots in this context. Finishing the analysis, the results are then displayed through histogram whereas the hotspot segments on the thermal image are marked with the segment box.

C. Development of Graphical User Interface for PV Module Extraction and Hotspot Detection Results Visualization

Fig.3 displays the plan of the graphical user interface. There are three frames in the main window, aligned horizontally to each other.

The first frame serves to hold the button widgets. A button named “choose dir” plays a role to let the user choose the path that save the images to be analyzed once the button is clicked. Another button named “choose save dir” allows user to decide the directory to store files. Besides, button “draw box” will create a new window displaying the current image to let user carry out manual operation for module extraction purpose in case of extraction failure.

The second frame serves to display the results of module extraction model to let the user see if there is any false detection. Also, two buttons named “<<” and “>>” can also be found in the second frame, allowing users to surf back and forth the directory storing the images so that the results of every image can be seen. Button “process” is also available to let user refresh the results once manual operation is to be executed.

The third frame displays the results of hotspot detection. The thermal image with hotspot segments highlighted will be shown. Meanwhile, the number of hotspots in that image can also be observed.

Several folders will also be created in the chosen directory to store the results. For instance, the bounding box coordinates, the module extraction, hotspot-highlighted images, and the histograms.

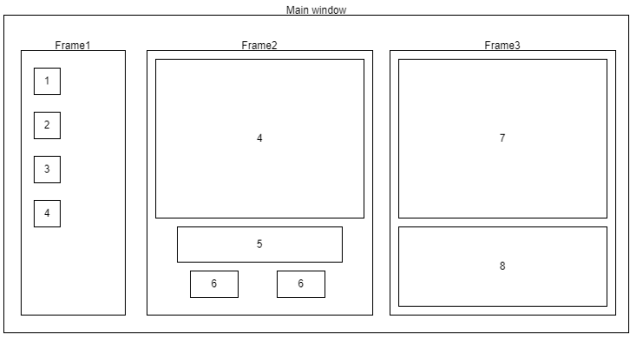

Fig.3. Graphical user interface.

III. RESULTS AND DISCUSSION

A. *Module Extraction*

A total of 88 images, thermal images and visual images reigning half of the number each, are taken for training purpose. Augmentation technique is applied to grow the database five times bigger, achieving 528 image numbers. Fig.4 shows the original images and their augmented images.

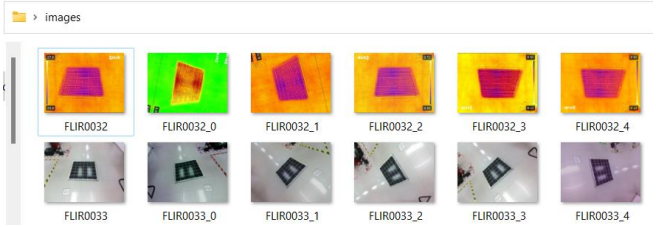

Fig.4. Original images and their augmented images.

Having the model trained, some unseen data is inputted and the results are tabulated. In TABLE I, 44 samples are taken for the experiment. 43 successful module extractions have been achieved, recording an accuracy of 98% with only 1 false negative detection failure. From the successful detections, it records a 95% confidence level of PV module recognition. 11% false positive detection is also recorded from the same experimental data. This high percentage may be caused by the overlapping of train set and validation set during the model training stage.

TABLE I. MODULE EXTRACTION RESULTS.

	Total	**Average**
Input Image	44	-
Module Detection	43	0.98
Confidence Level	-	0.95
False Negative	1	0.02
False Positive	5	0.11

B. *Hotspot detection*

Some thermal images are taken with the hotspots created at several positions. 44 images are successfully taken and used for analysis after the modules are extracted from the background. Fig.5 shows an example of the thermal image containing hotspot.

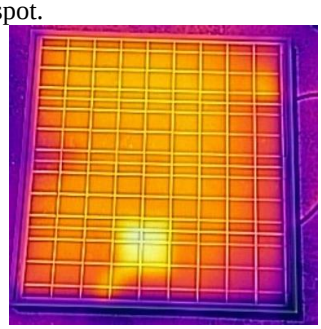

Fig.5. Thermal image containing hotspot.

Three image pre-processing steps are involved before the images are analyzed. Fig.6, Fig.7, and Fig.8 display the results of grayscale conversion, followed by contrast limited adaptive histogram equalization, and Gaussian blurring.

Fig.6. Grayscale conversion.

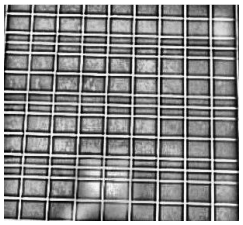

Fig.7. Application of contrast limited adaptive histogram equalization.

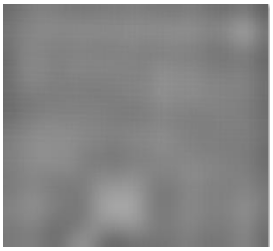

Fig.8. Gaussian blurring.

The pre-processed images are then segmented into 100 equal divisions. The segment box is imposed to the original thermal image in Fig.9.

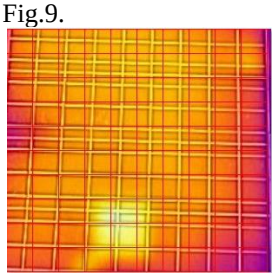

Fig.9. Image segmentation.

In the segmentation process, some pixel loss happens and the relevant data is tabulated as shown in TABLE II. It is observed that the module size in the sample images contains an average value of 108,029 pixels, ranging from 76372 pixels to 147,015 pixels. With the average 1,053 pixels segment size, ranging from 744 pixels to 1440 pixels, being applied to the sample images, an average loss of 2,738 pixels, which is equivalent to a 3% loss, is recorded. The maximum loss ratio is found to be 5% from sample image FLIR0282 with a module size of 100,224 pixels and a segment size of 952 pixels, recording a loss of 5,024 pixels.

TABLE II. SEGMENTATION STATISTICS.

	Average
Module Size (px)	108029
Segment Size (px)	1053
Pixel Loss (px)	2738
Loss Ratio	0.03

The segmented images are undergone statistical analysis by creating the upper boundary based on the sample median and standard deviation. The statistics are as shown in TABLE III. In the hotspot detection stage, a total of 286 hotspot segments are created in the sample images, with an average of 6.5 hotspot segments per sample. As a result, 232 hotspot segments are successfully detected from 44 sample images, recording an accuracy of 85%. On the other hand, a total of 32 false positive detections are also recorded, meaning that 0.73 false positive detections are observed in every sample image.

TABLE III. HOTSPOT DETECTION STATISTICS.

	Average
Actual Hotspot Number	6.5
Hotspot Detection	5.27
False Negative	1.23
False Positive	0.73
Accuracy	0.85

Table IV records the statistics in the hotspot detection stage. The average sample mean of the intensity value is found to be 132.37 whereas the sample median shows a value of 132.32. The sample means range from 128.89 to 134.36. Meanwhile, the average number of the sample standard deviation is 10.23, ranging from 6.35 to 12.37. Utilizing the median as well as the standard deviation, the upper boundary records an average value of 146.95, with its minimum value at 139.45 and its maximum value at 155.69. Besides, the mean hotspot values for all the sample images are also recorded with an average value of 158.48, having a minima of 144.08 and a maxima of 168.54.

TABLE IV. HOTSPOT DETECTION STATISTICS II.

	Average
Sample Mean	132.37
Sample Median	132.32
Sample Standard Deviation	10.23
Upper Boundary	146.95
Hotspot Mean Value	158.48

C. Graphical User Interface

A graphical user interface is created as planned, and it is shown in Fig.10. The first frame contains three buttons named “choose dir”, “choose save dir”, and “draw box” respectively. “Choose dir” button allows users to open the directory that stores the images to be analysed. “Choose save dir” button allows users to choose the directory to save the file. Meanwhile, “draw box” button, once clicked, will create a new window to let the user carry out manual operation in case of extraction failure.

The second frame displays the results of the module extraction after the directory is chosen. On top of the image, there are three buttons. “>>” and “<<” buttons serve to go back and forth once they are clicked. “Process” button is created in conjunction with “draw box” button. After manual extraction is carried out, “process” button can be clicked to refresh the hotspot detection results.

The third frame displays the hotspot-highlighted images that corresponds to the displaying image in the second frame. The hotspot number can also be found at the bottom right of the window.

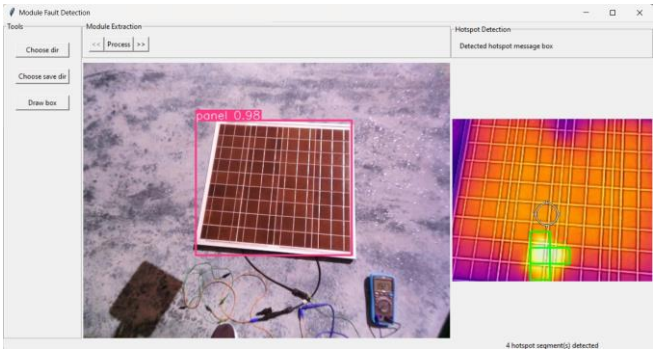

Fig.10. Graphical user interface.

D. Comparison

Looking at Table V, trained models reign high accuracy, ranging from 91.7% to 99%. Comparing the statistical method applied in this paper with these trained models, it may lose its competency with an accuracy of only 85%. However, one major advantage of applying the statistical method is that no large dataset is required as the prerequisite to build such a detection tool. Furthermore, the convenience of modifying the method may also be a highlight for this statistical method as the trained model needs to be re-trained prior to any change.

Comparing it with another image processing-based method, the statistical method in this paper contains higher accuracy of 85% whereas the adaptive thresholding contains an accuracy of 80% in the other paper.

TABLE V. COMPARISON OF HOTSPOT DETECTION ACCURACY USING DIFFERENT METHODS.

Hotspot Detection Method	**Accuracy**
Statistical analysis	85%
DCNN-based binary classification model [5]	99%
DCNN-based binary classification model(optimized) [5]	95.40%
DCNN-based multi-class classification model [5]	95.55%
DCNN-based multi-class classification model(optimized) [5]	90.80%
Resnet-50 [10]	97.85%
VGG-16 [10]	96.65%
Adaptive thresholding [7]	80%
YOLOv5 model [10]	91.70%
SVM-based machine learning model [11]	92.00%

Table VI displays the accuracies of different module extraction methods. The module extraction method in this paper is realised through the application of a customized YOLOv5 model and it achieves an accuracy of 98%. The module extraction method in the other paper applies an edge-detection-based algorithm which also reaches an accuracy of approximately 98%. Two method shows resemblance in terms

of accuracy, thus validating the competency of the method in this paper.

TABLE VI. COMPARISON OF MODULE EXTRACTION ACCURACY USING DIFFERENT METHODS.

Module Extraction Method	Accuracy
Customized YOLOv5 model	98%
Edge-detection-based algorithm [9]	97.90%

E. Limitations

Despite achieving the stated objectives, the process and the results of this paper encounter several confinements.

Firstly, the resolution of the image is restricted at the dimension of 640x480 pixels, influencing the quality of the results directly. The images that come with higher resolution would allow a better quality of analysis as more pixels are available for investigation. However, higher image resolution also requires more computing time, thus increasing the need for costly computing devices. Therefore, high image resolution turns out to be a double-edged sword.

Besides, the hotspots in this paper solely originate from shading by blocking the irradiance towards a certain part of the PV module using some opaque obstacles. Some other types of hotspots fail to be created and utilized in this paper due to limited resources.

Since there are only a limited amount of PV modules, the results of this paper are also confined to local hotspots. Furthermore, with the application of the statistical method to detect the hotspot, failure may be observed if the hotspot area turns out to be bigger or equivalent to the normal area as the distribution may be skewed.

Another limitation that can be found in this paper is that only one PV module will be extracted per image. However, the condition may be delimited by further modifying the code.

IV. CONCLUSION

As an encapsulation, this paper has successfully achieved the three stated objectives as mentioned in chapter one. The objectives revolve around detecting faults within modules using thermal imaging, creating an automated module extraction model, and creating a GUI to visualize the results.

To create an automated module extraction model, image collection for building the database is carried out using FLIR-Cx series thermal camera and a 50Wp PV module. Augmentation technique is applied to make up for the shortage of resources, increasing the size of database. Then, a customized module extraction model is trained based on the YOLOv5 algorithm, a machine learning model that help train a custom object detection model. 44 unseen sample images are then used to test the model accuracy. As the results, 43 modules out of 44 sample images have successfully been extracted, achieving an accuracy of 98%.

To detect fault within modules using thermal imaging, statistical method is applied to analyse the thermal image in this paper. segmentation is first implemented onto the module image in order to divide it into several pieces of samples. Each sample are calculated for their means. Then, sample mean, median, and standard deviation are calculated to set up the boundary in which those samples that lie outside of the boundary are deemed as outliers, also known as hotspot segments in this context. Consequently, hotspot detection using statistical analysis achieves an accuracy of 85%. This result is considered over the passing line as an image processing method to analyse hotspots.

The two mentioned stages are then studded into a GUI to visualize the results as shown in chapter 4. In the GUI, the user simply needs to open the directory that stores the images to be analysed, then the results for module extraction and hotspot detection will then be displayed after a few seconds of processing. Manual operation to extract the PV module is also available for the user in case of extraction failure.

Eventually, the three stated objectives in this paper are emphasized and realised through the planned methodology with the desired results displayed in previous chapters.

ACKNOWLEDGEMENT

Million thanks to those who have been providing technical support and guiding me all the way along the progress of this study especially the staff from School of Electrical and Electronic Engineering, Universiti Sains Malaysia.

Besides, words alone could not describe the gratitude that I would like to express to my beloved family who have never fail to support me physically, emotionally and financially.

REFERENCES

[1] O. W. I. Data, "Share of electricity production from renewables, 2022," Our World In Data, [Online]. Available: https://ourworldindata.org/grapher/share-electricity-renewables. [Accessed 30 January 2023].

[2] IEA, "Executive summary," IEA, 2022. [Online]. Available: https://www.iea.org/reports/renewables-2021/executive-summary. [Accessed 30 January 2023].

[3] Kuby, "The Positive and Negative Environmental Impacts of Solar Panels," Kuby Renewable Energy Ltd., [Online]. Available: https://kubyenergy.ca/blog/the-positive-and-negative-environmental-impacts-of-solar-panels. [Accessed 30 January 2023].

[4] A. Mellit, "An embedded solution for fault detection and diagnosis of photovoltaic modules using thermographic images and deep convolutional neural networks," *Engineering Applications of Artificial Intelligence*, vol. 116, p. 105459, 2022.

[5] Moath Alsafasfeh, Ikhlas Abdel-Qader, Bradley Bazuin, "Fault Detection in Photovoltaic System Using SLIC and Thermal Images," in *International Conference on Information Technology (ICIT)*, Michigan, 2017.

[6] Luis E. Montanez, Luis M. Valent´ın-Coronado, Daniela Moctezuma, Gerardo Flores, "Photovoltaic module segmentation and thermal analysis tool from thermal images," in *2020 IEEE International Autumn Meeting*, Ixtapa, 2020.

[7] Masoud Alajm, Khalfalla Awedat, Mohammed Sharaf Aldeen, Salman Alwagdani, *IR Thermal Image Analysis: An Efficient*

Algorithm for Accurate Hot-Spot Fault Detection and Localization in Solar Photovoltaic Systems, Taif: Taif University, 2019.

[8] Xiang Gao, Eric Munson, Glen P. Abouslemen, Jennie Si, "Automatic solar panel recognition and defect detection using infrared imaging," in *SPIE*, Tempe, 2015.

[9] Feng Hong, Jie Song, Hang Meng, Rui Wang, Fang Fang, Guangming Zhang, "A novel framework on intelligent detection for module defects of PV plant combining the visible and infrared images," *Solar Energy*, vol. 236, pp. 406-416, 2022.

[10] Muhammad Umair Ali, Hafi Farhaj Khan, Manzar Masud, Karam Dad Kallu, Amad Zafar, "A machine learning framework to identify the hotspot in photovoltaic module using infrared thermography," *Solar Energy*, vol. 208, pp. 643-651, 2020.

[11] Roberto Pierdicca, Marina Paolanti, Andrea Felicetti, Fabio Piccinini, Primo Zingaretti, "Automatic Faults Detection of Photovoltaic Farms: solAIr, a Deep Learning-Based System for Thermal Images," *MDPI Energies*, vol. 13, p. 6496, 2020.